Supramolecular assembly of biological molecules purified from bovine nerve cells: from microtubule bundles and necklaces to neurofilament networks



2005 J. Phys.: Condens. Matter 17 S3225

(http://iopscience.iop.org/0953-8984/17/45/005)

INSTITUTE OF PHYSICS PUBLISHING JOURNAL OF PHYSICS: CONDENSED MATTER

J. Phys.: Condens. Matter **17** (2005) S3225–S3230 doi:10.1088/0953-8984/17/45/005

# Supramolecular assembly of biological molecules purified from bovine nerve cells: from microtubule bundles and necklaces to neurofilament networks

**Daniel J Needleman[1], Jayna B Jones[1], Uri Raviv[1], Miguel A Ojeda-Lopez[1], H P Miller[2], Y Li[1], L Wilson[2] and C R Safinya[1]**

[1] Materials Department, Physics Department, Molecular, Cellular, and Developmental Biology Department, University of California, Santa Barbara, CA 93106, USA
[2] Molecular, Cellular, and Developmental Biology Department and Biomolecular Science and Engineering Program, University of California, Santa Barbara, CA 93106, USA

E-mail: safinya@mrl.ucsb.edu

Received 7 October 2005
Published 28 October 2005
Online at stacks.iop.org/JPhysCM/17/S3225

**Abstract**

With the completion of the human genome project, the biosciences community is beginning the daunting task of understanding the structures and functions of a large number of interacting biological macromolecules. Examples include the interacting molecules involved in the process of DNA condensation during the cell cycle, and in the formation of bundles and networks of filamentous actin proteins in cell attachment, motility and cytokinesis. In this proceedings paper we present examples of supramolecular assembly based on proteins derived from the vertebrate nerve cell cytoskeleton. The axonal cytoskeleton in vertebrate neurons provides a rich example of bundles and networks of neurofilaments, microtubules (MTs) and filamentous actin, where the nature of the interactions, structures, and structure–function correlations remains poorly understood. We describe synchrotron x-ray diffraction, electron microscopy, and optical imaging data, in reconstituted protein systems purified from bovine central nervous system, which reveal unexpected structures not predicted by current electrostatic theories of polyelectrolyte bundling, including three-dimensional MT bundles and two-dimensional MT necklaces.

(Some figures in this article are in colour only in the electronic version)

## 1. Introduction

With the emerging proteomics era, the biosciences community is now challenged to elucidate the structures and functions of a large number of interacting proteins. Cellular activity, which

is tightly regulated, is often a result of protein–protein and protein–nucleic acid interactions, which may lead to the formation of assemblies of biomolecules for distinct functions. Our understanding of modern biology has to a significant degree resulted from our knowledge of the structures of biological molecules, which may provide direct information relating to function. The elucidation of *in vitro* supramolecular structures—spanning length scales from nanometres to microns—designed to model *in vivo* conditions of interacting proteins required for cell function will require interdisciplinary approaches and techniques. An important goal in biophysics is the understanding of interactions leading to supramolecular structures of cytoskeletal proteins and associated biomolecules, and most important the elucidation of the roles the structures play in cell functions.

We briefly describe an example from the nerve cell cytoskeleton, which shows a rich variety of poorly understood distinct structures, from single microtubules to networks and bundles of microtubules and neurofilaments, and motivates us to understand the physics of their assembly reconstituted, *in vitro*, from purified protein. Two interacting nerve cells are shown schematically in figure 1 (top). Figure 1 (lower left) shows an electron micrograph of a longitudinal cut along a nerve cell axon, which exposes the axonal cytoskeleton [1]. One microtubule (MT, red arrow) is visible near the middle with attached vesicles. Here, the MT provides a track for the transport of organelles (for example, vesicles, which may contain precursor molecules of neurotransmitters required for nerve cell signal transduction), towards an axon–dendrite or axon–cell body synapse (cartoon in figure 1). In figure 1 (lower right) the electron micrograph shows a section near the initial axon segment near the cell body [2]. A finite sized bundle of MTs is clearly visible (large white arrow). MT bundles are thought to be stabilized by microtubule-associated proteins (MAPs), which non-covalently cross-link neighbouring MTs through a combination of electrostatic, hydrogen bonding, and possible hydrophobic interactions (thin, white arrow).

In Alzheimer's disease the chemically altered MAP tau protein (thin white arrow in figure 1, lower right) unbinds from microtubules, which disrupts the MT stability and bundle assembly and inhibits material transport along axons. The role of MT bundles in nerve cells is not understood. In particular, the parameters which determine the bundle size and the nature of MT assembly remain to be elucidated. As we describe, our experiments with reconstituted MT and bundle-inducing counter-ions show that the charge of the counter-ion is a key experimental parameter controlling the bundle size and unexpectedly the structure and symmetry of the assembly.

In both images the single MT (figure 1 lower left) and the MT bundle (figure 1 lower right) are surrounded by a network of neurofilaments (NFs, red stars), which play a major role in the structural stability of the axon of vertebrate nerve cells. Neurofilaments are heteropolymers consisting of three distinct molecular weight fractions labelled NF-L, NF-M, and NF-H (see figures 2(A) and (B)). Upon reconstitution, purified NF fractions spontaneously assemble to form a core filamentous protein and long carboxy side-arms, which extend away from the overall negative charged NF filament (figure 2(A)). The micrographs in figure 1 show the cross-bridging between neighbouring neurofilaments resulting from side-arm interactions. A known hallmark of motor neuron diseases such as amyotrophic lateral sclerosis is the disruption of the NF network due to incorrect side-arm interactions [3].

## 2. Experimental details, results and discussion

The nature of neurofilament self-assembly in reconstituted systems is poorly understood. Our recently purified and reconstituted NFs form a liquid crystalline gel phase (figure 2(B)). This is seen in polarized microscopy images in figure 2(C), where the texture is characteristic of

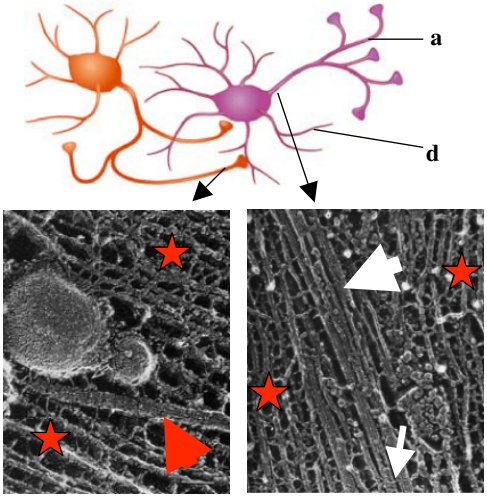


**Figure 1.** Top: sketch of two interacting nerve cells (a = axon, d = dendrite). The axon of the cell on the left is forming synaptic junctions with the cell body and dendrite of the cell on the right. Lower left: electron micrograph of a mouse nerve axon showing a single microtubule (MT, red arrow) with a vesicle moving along the MT surrounded by neurofilaments (NFs, red stars). Adapted from [1]. Lower right: electron micrograph of a frog spinal nerve. A microtubule bundle is seen (large white arrow) embedded within the NF network (red stars). Microtubule-associated proteins (tau protein, thin white arrow) non-covalently cross-link the MTs. Adapted from [2]. Micrographs are from Hirokawa. In these images the diameter of an individual MT is 25 nm.

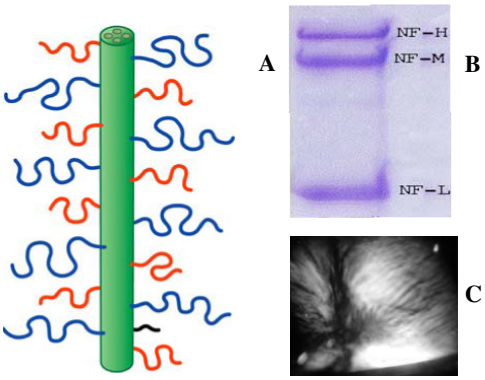


**Figure 2.** (A) Schematic diagram of a neurofilament (NF) showing the side-arms of NF-H (blue), NF-M (red), and NF-L (black) fractions containing 600, 500, and 150 amino acid residues respectively. (B) Gel electrophoresis pattern (10% polyacrylamide in sodium dodecyl sulfate) of purified neurofilaments (NFs) showing the three fractions (NF-L, MW = 60 K; NF-M, MW = 100 K; NF-H, MW = 115 K). NFs purified from bovine spinal chord according to the procedures described in [5], and modified in [6] and [7]. (C) A typical reconstituted NF mixture viewed between crossed polarizers shows the presence of nematic-like liquid crystalline texture.

a nematic *liquid crystalline* network with long-range orientational order associated with the filamentous network. The precise nature of short-range and long-range interactions between NFs resulting from side-arm interactions remains mostly controversial, primarily due to the lack of quantitative data. Small-angle x-ray scattering data from reconstituted neurofilament mixtures shows the promise of beginning to reveal the nature of the side-arm interactions in controlling the inter-filament interactions [4].

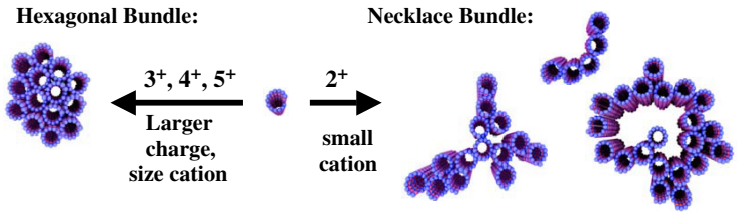


**Figure 3.** Three-dimensional schematics of higher-order assembly of nanometre-scale microtubules. Left: larger sized trivalent (spermidine $[H_3N^+–(CH_2)_3–^+NH_2–(CH_2)_4–^+NH_3]$, $lysine_3$), tetravalent (spermine $[H_3N^+–(CH_2)_3–^+NH_2–(CH_2)_4–^+NH_2–(CH_2)_3–^+NH_3]$, $lysine_4$), and pentavalent ($lysine_5$) cations lead to the formation of tight hexagonal bundles. Right: small sized divalent cations $[(Ba^{2+}, Ca^{2+}, Sr^{2+})]$ lead to the necklace bundles with linear, branched, and loop morphologies. Adapted from [8].

In recent experiments we have explored the assembly behaviour of microtubules (MTs), a cytoskeletal polymer and model nanoscale tubule, and multivalent cations [8]. The experimental details are described in detail in [8, 9]. Tightly packed hexagonal bundles with controllable diameters are observed for large tri-, tetra-, and pentavalent counterions (cartoon on left side in figure 3). Unexpectedly, in the presence of small divalent cations, we have discovered a living necklace bundle phase, comprised of dynamical assemblies of MT nematic membranes with linear, branched, and loop topologies (cartoon on right side of figure 3). The morphologically distinct MT assemblies give insight into general features of bundle formation and may be used as templates for miniaturized materials with applications in nanotechnology and biotechnology.

The structure of these supramolecular assemblies was elucidated on length scales from subnanometre to micrometre with synchrotron x-ray diffraction, transmission electron microscopy, and differential interference contrast microscopy.

The mesoscopic structure of MT bundles is shown in video-enhanced DIC images of figure 4(A). The bundles formed in the presence of large, tri-, tetra-, and pentavalent cations, (such as $spermine^{4+}$) appear thick and curved, while bundles formed with small divalent cations (such as $Ba^{2+}$) are straight. Individual MTs can be resolved with TEM, which clearly shows that bundles formed with large multivalent ions are thick, with MTs tightly packed into a hexagonal array (figure 4(B)). A radically different bundle structure, which we refer to as the living necklace bundle phase of MTs, is observed when the condensing ions are small, divalent cations. On the nanometre scale, TEM shows that these necklace bundles are highly flexible in cross-section, giving rise to topologically distinct linear, branched, and loop morphologies (figure 4(C)).

We have performed a series of synchrotron small-angle x-ray scattering and diffraction (SAXRD) experiments at the Stanford Synchrotron Radiation Laboratory (SSRL) on beamline 4-2 to gain further insight into the ångström scale structure of these MT bundles. Figure 5(A) shows representative raw SAXRD scans that have been integrated over 360° from a powder pattern on a 2D detector, and are displayed as a function of the scattering vector, $q$.

To quantitatively model these data, we have subtracted a background that consists of a polynomial that passes through the minimum of the scattering intensities (figure 5(B)). The MTs are modelled as hollow cylinders with an outer radius of 12.9 nm and a wall thickness of 3.2 nm (figure 5(B), labelled 'No Cation'). The tight bundle phase, for ions with valence five to three, are modelled as a collection of hollow cylinders, with the dimensions given above, packed into a hexagonal lattice. These bundles are finite-size, hexagonal, columnar liquid crystals [10]. The average bundle thickness can be determined from the peak width using

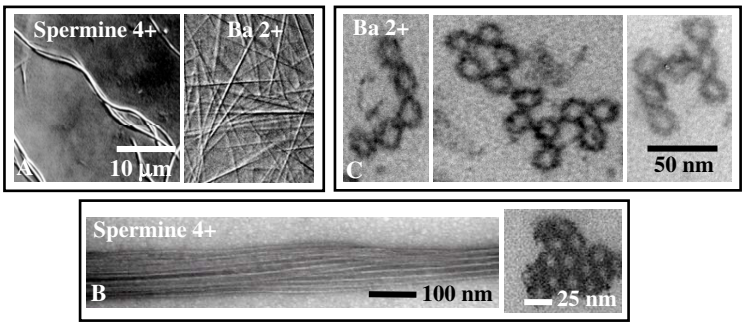


**Figure 4.** (A) Differential interference contrast (DIC) optical micrographs of hexagonal microtubule (MT) bundles with 4+ (5 mM spermine) and 2+ (100 mM $BaCl_2$). (B) (left) whole mount TEM side view of hexagonal MT bundles (10 mM spermine) and (right) plastic embedded TEM cross section. (C) Plastic embedded TEM cross sections of bundles with 100 mM $BaCl_2$ showing (left) linear, (centre) loop-like and (right) branched morphologies. Adapted from [8].

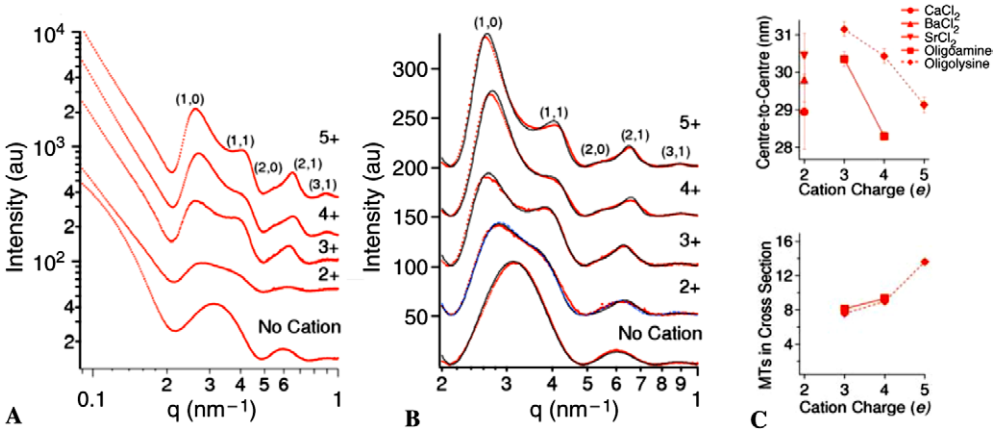


**Figure 5.** (A) Raw SAXRD scattering data for MTs with no cation, (2+) 115 mM $BaCl_2$, (3+) 15 mM spermidine, (4+) 5 mM spermine, or (5+) 5 mM oligolysine-five with hexagonal bundle peaks indexed. (B) Data in (A) after background subtraction (dots) with fitted model scattering curves (lines). (C) Summary of SAXRD scattering fit parameters of MT bundles with $CaCl_2$, $SrCl_2$, $BaCl_2$, oligoamines (spermidine and spermine), and oligolysines. Adapted from [8]. The critical concentration for the onset of bundles is 60 ± 10 mM for Ba (2+), 40 ± 10 mM for Ca (2+), 7.5 ± 1.5 mM for spermidine (4+), 1.5 ± 1 mM for spermine (3+), and 0.75 ± 0.25 for oligolysine-five (5+).

Warren's approximation [11]. As the charge of the condensing ion decreases from $5^+$ to $4^+$ to $3^+$ the MT centre-to-centre distance increases and the bundle size decreases (figure 5(C)). SAXRD scans of bundles assembled with divalent ions display very broad peaks (figure 5(A), $2^+$), in contrast with the tight bundle phase. Indeed, instead of the hexagonal bundles observed with larger multivalent ions, detailed analysis shows that these SAXRD data can be quantitatively modelled as arising from a dimer of MTs. The only fit parameter is the MT–MT spacing (figure 5(C), top, $Ca^{2+}$, $Ba^{2+}$, $Sr^{2+}$). The SAXRD data combined with TEM results (figure 4(C)) show that these living bundles are finite size, locally two-dimensional membranes with nematic ordering, i.e. they consist of rod-like subunits (MTs) that spontaneously break symmetry by orienting but show only short-range positional order. These bundles are an experimental

realization of nematic membranes which have recently been predicted as a new universality class of membrane [12].

Much remains to be studied about the precise nature of supramolecular assemblies of neurofilaments and microtubules and the conditions which lead to the formation of different types of bundles with distinct symmetries and structures [4, 8, 9, 14, 15]. For example, while a large number of key proteins have been identified through molecular biology and genetics studies as being critical to the overall stability of the axonal cytoskeleton, we still have very little knowledge of the supramolecular structures which are assembled when the cytoskeleton of the nerve cell is constructed and dynamically repaired throughout life. The model system studied here may be viewed as a step toward understanding how varying microscopic interactions lead to the wide variety of MT bundles observed *in vivo* [2, 13]. In addition to providing insight into the fundamental physics of rod-like polyelectrolytes and the general determinants of bundle structure, the control of bundle morphology demonstrated here may help to assemble nanostructures for engineering and biomedical applications.

## Acknowledgments

The authors acknowledge support by NIH GM-59288 and NS-13560, and NSF DMR-0503347 and CTS-0404444. UR acknowledges Fellowship support from the International Human Frontier Science Program and the European Molecular Biology Organizations. The x-ray scattering studies were carried out at the Stanford Synchrotron Radiation Laboratory, a national user facility operated by Stanford University on behalf of the US Department of Energy, Office of Basic Energy Sciences.

## References

[1] Hirokawa N 1996 *Trends Cell Biol.* **6** 135–41
[2] Peters A, Palay S L and Webster H D E F 1991 *The Fine Structure of the Nervous System* 3rd edn (New York: Oxford University Press)
[3] Miller C C J, Ackerley S, Brownlees J, Grierson A J, Jacobsen N J O and Thornhill P 2002 *Cell. Mol. Life Sci.* **59** 323–30
[4] Jones J B, Ojeda-Lopez M and Safinya C R 2005 in preparation
[5] Leterrier J F and Eyer J 1987 *Biochem. J.* **245** 93–101
[6] Leterrier J F, Käs J, Hartwig J, Vegners R and Janmey P A 1996 *J. Biol. Chem.* **271** 15687–94
[7] Liem R K 1986 **134** 384–8
[8] Needleman D J, Ojeda-Lopez M A, Raviv U, Miller H P, Wilson L and Safinya C R 2004 *Proc. Natl Acad. Sci. USA* **101** 16099–103
[9] Raviv U, Needleman D J, Li Y, Miller H P, Wilson L and Safinya C R 2005 *Proc. Natl Acad. Sci. USA* **102** 11167–72
[10] Selinger J V and Bruinsma R F 1991 *Phys. Rev.* A **43** 2910–21
[11] Warren B E 1941 *Phys. Rev.* **59** 693–8
[12] Xing X, Mukhopadhyay R, Lubensky T C and Radzihovsky L 2003 *Phys. Rev.* E **68** 021108
[13] Bray D 2001 *Cell Movements* (New York: Taylor and Francis)
[14] Needleman D J, Ojeda-Lopez M A, Raviv U, Ewert K, Jones J B, Miller H P, Wilson L and Safinya C R 2004 *Phys. Rev. Lett.* **93** 198104-1–4
[15] Tang J X and Janmey P A 1996 *J. Biol. Chem.* **271** 8556–63